SUSTAINABLE RESIDENTIAL POWER: HYBRID INVERTERS FOR ON/OFF-GRID FLEXIBILITY

Israel Dourado[1], Ernande E. C. Morais[1] and Dalton de A. Honorio[1]

[1] Federal University of Ceará, Fortaleza (Brazil)

Abstract

This paper presents a hybrid single-phase inverter with dual operational modes, designed to enhance the resilience of residential microgrids by enabling seamless transitions between grid-connected and off-grid operation. Targeting 4 kW power applications, the inverter employs a full-bridge topology with an LCL filter and is digitally controlled. In On-Grid mode, it synchronizes with the utility grid via a Phase-Locked Loop (PLL), injecting surplus renewable energy and maintaining power quality. During grid outages (Off-Grid mode), it operates as a Voltage Source Inverter (VSI), establishing a stable local grid to power residential loads. By integrating renewable energy utilization, battery storage, and adaptive digital control, the design addresses technical challenges such as reduced grid inertia and regulatory barriers to distributed generation. This solution empowers homeowners with energy autonomy, reduces carbon emissions, and enhances grid resilience, positioning hybrid inverters as key enablers of sustainable, decentralized power systems.

Keywords: Residential Microgrids, Hybrid Inverter, Grid-Forming Inverter (GFM), Grid-Following Inverter (GFL), Renewable Energy Systems (RES)

1. Introduction

Climate change, environmental impact, financial aspects, and natural resources are often the foundational pillars driving the quest for technological innovation in the energy sector. Global energy demand is accelerating, which not only depletes fossil fuel reserves but also hurts the environment. It is increasingly recognized that renewable energy sources, such as photovoltaic solar and wind power, can offer effective solutions to the immense challenge of meeting global energy demand without harming the environment [1], [2]. To provide some context, a single 10MW photovoltaic power plant prevents the release of approximately 15,000 tons of CO2 into the atmosphere annually, which would otherwise result from burning fossil fuels [3].

In the pursuit of more sustainable solutions, the electrical sector has undergone profound transformations in recent years. The traditional centralized generation/transmission system, where electricity is produced in large, often remote power plants requiring extensive transmission lines to reach consumption centers, is being progressively replaced by what is known as Distributed Generation (DG) [4], [5]. The development of new technologies, particularly photovoltaic panels, has contributed massively to this decentralization [6], [7].

With the increasing integration of grid-connected power electronic converters, predominantly of the grid-following type, certain issues—previously well-managed by traditional synchronous generators—have begun to emerge in electrical networks as the penetration rate of these converters rises, namely:

1) The problem of reduced grid inertia. In traditional systems, the rotational speed of synchronous machines determines the grid frequency, and the slow dynamic response of these machines contributes to frequency stability.
2) The transient response speed of the grid voltage and frequency. Electronic converters exhibit a fast dynamic response, in contrast to the slower response of synchronous generators [8], [9].

This means that, depending on the penetration level, instabilities in grid voltage and/or frequency can be induced [10]. Furthermore, with the increased installation of these systems directly interconnected with the local utility grid, various technical and bureaucratic barriers have been raised by utility companies aiming to restrict access to their networks.

Due to these challenges, and with recent advances in energy storage battery technology, a potential solution is

10.18086/swc.2025.07.14 Available at http://proceedings.ises.org

for the end consumer to store this excess energy, thereby preventing waste and utilizing it at a more convenient time [4], [10].

Within this context, the concept of residential microgrids is gaining traction and emerging as a trend for the near future. In this setup, multiple generation sources are connected to a common bus, share their generated power, and any surplus energy is either fed back to the local utility grid or stored in a battery bank [11], [12]. Figure 1(a) below shows the topology of a residential DC microgrid with a common DC bus and a hybrid grid-forming/grid-following inverter, while Figure 1(b) presents the power topology choose as the inverter.

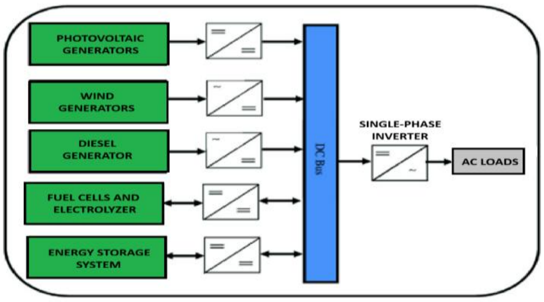

Figure 1(a): LCL Filter with Resistor in Parallel with Capacitor

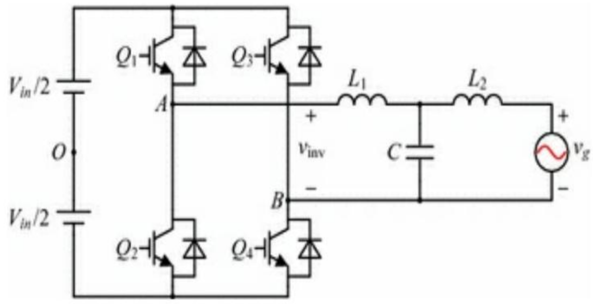

Figure 1(b): Comparison between an LCL filter with and without resonance damping

2. LCL Filter Resonance Frequency

Control challenges for grid-tied inverters with an LCL filter arise from the resonance problem. At the resonant frequency, the LCL filter resonance causes an abrupt phase shift of -180 degrees with a high magnitude peak. This magnitude peak easily drives the system towards instability and must be damped.

Among the basic passive damping solutions, adding a resistor in parallel with the capacitor demonstrates the best damping performance, but this results in high power loss. To avoid power dissipation in the damping resistor, active damping solutions are equivalent to having a virtual resistor in parallel with the capacitor. The active damping method based on capacitor current feedback is superior due to its simple implementation and effectiveness.

By representing the inverter bridge's output voltage as a voltage source, we obtain the equivalent circuit of the LCL filter shown in Figure 1(b).

The dynamic equations of the equivalent circuit are shown below:

$$\begin{cases} i_1(s) = \dfrac{v_{inv}(s) - v_C(s)}{L_1.s} & (i) \\ i_C(s) = \dfrac{v_C(s)}{\dfrac{1}{C.s}} = v_C(s).C.s & (ii) \\ i_2(s) = \dfrac{v_C(s)}{L_2.s} \Rightarrow v_C(s) = i_2(s).L_2.s & (iii) \\ i_1(s) = i_C(s) + i_2(s) & (iv) \end{cases}$$

The transfer function for the grid current can be obtained as follows (considering the source to be zero):

$$G_{LCL} = \frac{i_2(s)}{v_{inv}(s)} = \frac{1}{s.L_1.L_2.C} \cdot \frac{1}{s^2 + \left(\sqrt{\dfrac{L_1 + L_2}{L_1.L_2.C}}\right)^2}$$

From this transfer function, we obtain that the resonance frequency of the inverter LCL filter is given by:

$$\omega_r = \sqrt{\frac{L_1 + L_2}{L_1.L_2.C}} \Rightarrow f_r = \frac{1}{2\pi} \cdot \sqrt{\frac{L_1 + L_2}{L_1.L_2.C}}$$

3. LCL Filter Design

The LCL filter of the inverter was designed based on its operation in grid-following mode. The design of the inverter's LCL filter incorporates the following required inverter characteristics, such as nominal power equals 4 kW, nominal main rms voltage equals 220V with peak in 311,13 V, power grid frequency equals 60 Hz, switching frequency equals 25 kHz, DC Bus voltage equals 400 V, and the modulation methodology applied is SPWM SINGLE POLAR.

Figure 2(a) below shows a zoom in on the unipolar SPWM waveforms. i_{1f} is the fundamental component of the inverter-side i_1 is the inductor current, and T_{SW} is the period of the triangular carrier.

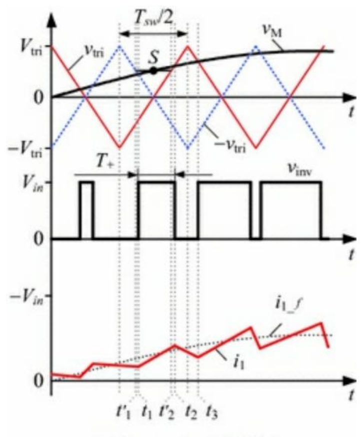

Figure 2(a): SPWM single-polar

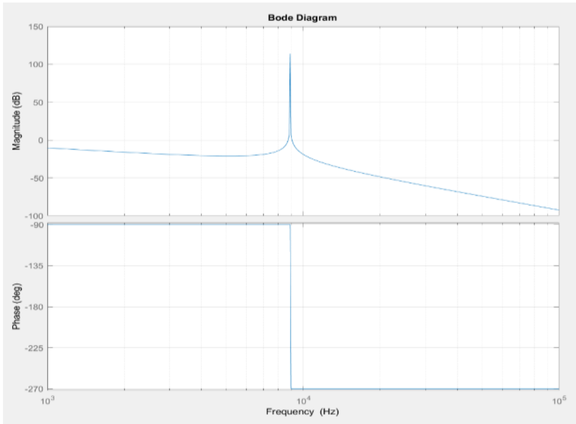

Figure 2(b): Bode Diagram of the LCL Filter.

3.1. Inductance, L1

$$\begin{cases} L_1 = \dfrac{V_{BUS}}{8.f_{SW}.\lambda_{c\_L1}.I_{1(RMS)}} \\ L_{1(máx)} \approx \dfrac{\lambda_{v\_L1}.V_g}{I_{1(RMS)}.\omega_o} \end{cases}$$

Where l_{cL1} denotes the percentage of ripple current in the inductor in relation to the effective current value (in our project, we adopted 20%), l_{vL1} denotes the percentage of voltage drop across L_1 (here adopted at 5%):

$$\begin{cases} V_{IN} = 400V \\ V_g = 220V \\ f_{SW} = 25\,kHz \\ \lambda_{c\_L1} = 20\% \\ \lambda_{v\_L1} = 5\% \\ I_{1(RMS)} = 18{,}18A \\ \omega_o = 2.\pi.f_o = 377\,rad/s \end{cases} \Rightarrow L_1 = 550\mu H$$

3.2. Capacitance, C

The filter capacitor will inject reactive power. The higher the capacitance, the more reactive power is introduced, and the greater the current flows through inductor L_1 and the power switches. Therefore, conduction losses in the switches will also increase. Let's define l_C as the ratio of the reactive power introduced by the filter capacitor to the nominal active power of the inverter connected to the grid. Thus:

$$\lambda_C = \frac{Q_C}{P_{out}} \Rightarrow \lambda_C = \frac{\left(\dfrac{V_g^{\,2}}{X_C}\right)}{P_{out}} \Rightarrow \lambda_C = \frac{\omega_o.C.V_g^{\,2}}{P_{out}} \Rightarrow C = \frac{\lambda_C.P_{out}}{\omega_o.V_g^{\,2}}$$

In practice, λ_C is usually recommended to stay around 5%. This replaces the values previously assigned.

$$C = \frac{\lambda_C.P_{out}}{\omega_o.V_g^{\,2}} \Rightarrow C = \frac{5\%.4000}{377.220^2} \Rightarrow C = 10{,}96\mu F$$

3.3. Inductance, L2

For the harmonic w_h of interest, we have that:

$$G_{LCL}(j.\omega_h) = \frac{i_2(j.\omega_h)}{v_{inv}(j.\omega_h)} = \frac{1}{L_1.L_2.C.(j.\omega_h)^3 + j.\omega_h.(L_1+L_2)} \Rightarrow L_2 = \frac{1}{L_1.C.\omega_h^2 - 1}.\left(L_1 + \frac{|V_{inv}(j.\omega_h)|}{\omega_h.|i_2(j.\omega_h)|}\right)$$

The desired harmonic current can be expressed as a percentage of the nominal effective current value injected into the network, i.e., by defining $\lambda_h = \frac{|i_2(j.\omega_h)|}{I_{2(RMS)}}$, where $|V_{inv}(j.\omega_h)|$ is the effective value of the h-th harmonic of the output voltage, and is the effective value of the current injected into the grid. Since the desired harmonic order is greater than 33, we must have such a harmonic current less than 0.3% of the nominal current. Therefore, we will choose this ratio to be 0.2%: $\lambda_h = 0.2\%$.

For the frequency considered, we have that $\frac{|V_{inv}(j.\omega_h)|}{V_{IN}} = 24.7\% \Rightarrow |V_{inv}(j.\omega_h)| = 98.99V$. So, we can now find the value of L_2:

$$\begin{cases} L_1 = 550\mu H \\ C = 10,96\mu F \\ \omega_h = 2.\pi.50040 \\ \lambda_h = 0,2\% \\ I_{2(RMS)} = 18,18A \\ |V_{inv}(j.\omega_h)| = 98,99V \end{cases} \Rightarrow L_2 = \frac{1}{L_1.C.\omega_h^2 - 1}.\left(L_1 + \frac{|V_{inv}(j.\omega_h)|}{\omega_h.\lambda_h.I_2}\right) \Rightarrow L_2 = 15.48\mu H$$

Thus, the parameters of the LCL filter are: L1 = 550 μH, L2 = 15.48 μH, and C = 10.96 μF.

3.4 LCL Filter Resonance Frequency:

$$f_r = \frac{1}{2\pi}.\sqrt{\frac{L_1 + L_2}{L_1.L_2.C}} \Rightarrow f_r = 12,390\ Hz$$

Figure 2(b) shows the Bode plot of the LCL filter.

4. Resonance Damping

Active damping using state-variable feedback is a method that uses feedback from a suitable state variable to simulate a virtual resistor instead of a physical resistor. A resistor in parallel with a capacitor is the passive damping method with the best damping performance. Thus, active damping solutions that are equivalent to a resistor in parallel with a capacitor have the same damping performance without power losses. Figure 3(a) shows the LCL filter with an R_{C2} resistor parallel with the filter capacitor.

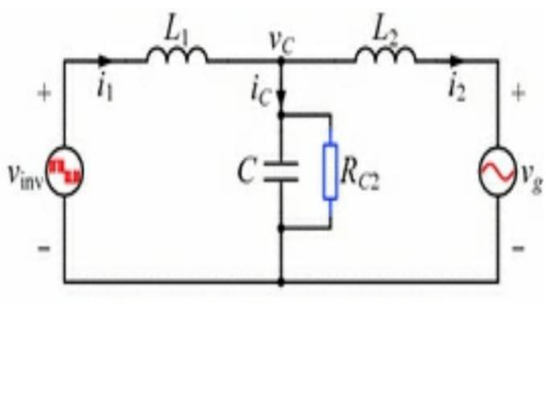

Figure 3(a): LCL Filter with Resistor in Parallel with Capacitor

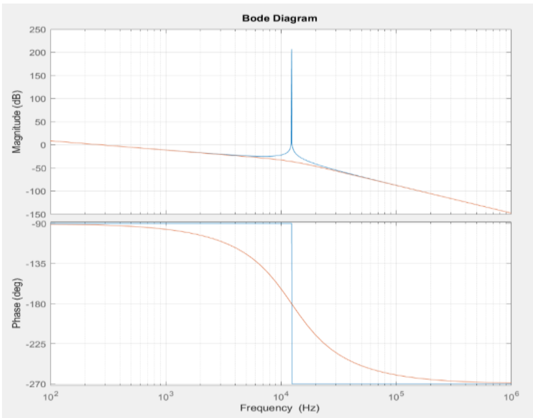

Figure 3(b): Comparison between an LCL filter with and without resonance damping.

According to [13], capacitor current feedback with a gain of $H_{i1} = \left(\frac{L_1}{K_{PWM}.C.R_{C2}}\right)$ is equivalent to having a resistor R_{C2} in parallel with capacitor C, where K_{PWM} denotes the gain of the PWM modulator. In this case, there is no power dissipation, thus configuring an active method of resonance damping. Figure 3(b) shows the effect of damping on the LCL filter. We can see that at frequencies below and above the resonance frequency, the filter behaved the same way, and at resonance, the peak was clipped (damped).

5. Inverter Modeling

The proposed inverter operates in two modes: Grid Follower and Grid Former. Table 1 presents the nominal and full-scale parameters for sizing the inverter control loops.

Table 1 – Full Scale Parameters for Inverter Modeling.

PARAMETERS FOR CONTROL LOOPS	
NOMINAL POWER OF THE INVERTER	4 kW
RATED OUTPUT CURRENT	18.18 A
NOMINAL OUTPUT RMS VOLTAGE	220 V
DC BUS NOMINAL VOLTAGE	400 V
INJECTED FULL-SCALE CURRENT	50 A
CURRENT SENSOR GAIN H_{i2}	0,02
OUTPUT FULL-SCALE VOLTAGE	400 V
VOLTAGE SENSOR GAIN	0.0025

In this section, we will present the modeling of the inverter in grid follower mode. The inverter topology with its control is shown in Figure 4(a).

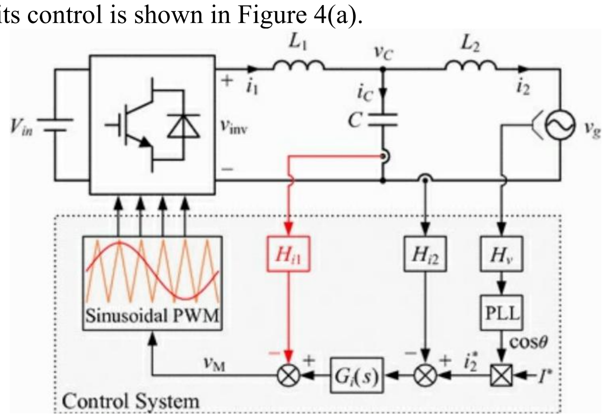

Figure 4(a): Grid Follower Inverter Topology

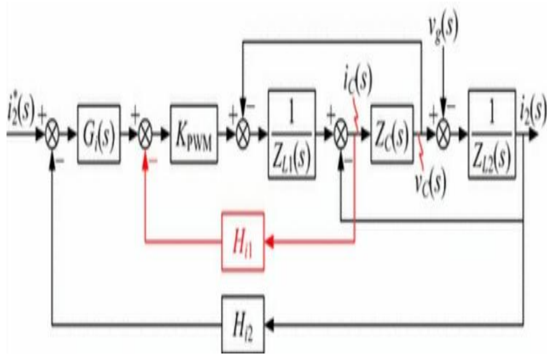

Figure 4(b): Block Diagram of Single-Phase Inverter Operating in Grid Follower Mode

The block diagram of the inverter is shown in Figure 4(b). The open-loop transfer function of the converter is given by:

$$FTMA(s) = \frac{H_{i2}.K_{PWM}.G_i(s)}{s^3.L_1.L_2.C + s^2.L_2.C.H_{i1}.K_{PWM} + s.(L_1 + L_2)}$$

Figure 5(a) shows the frequency response of the uncompensated system.

Next, we have the design procedure for the PR regulator, whose main advantage over the traditional PI regulator is the ability to provide a high gain at the desired grid frequency, T_{fo}, which reduces the steady-state error. To preserve a certain adaptability to the grid frequency, a practical alternative PR regulator is shown below:

$$G_i(s) = K_P + \frac{2.K_r.\omega_i.s}{s^2 + 2.\omega_i.s + \omega_o^2}$$

Where is the proportional gain, K_r, is the resonant gain, $\omega_o = 2.\pi.f_o$ is the fundamental angular frequency, and ω_i is the bandwidth of the resonant part (with a -3dB drop relative to the cutoff frequency), which means that the gain of the resonant part is in $\left(\frac{K_r}{\sqrt{2}}\right)$ in $(\omega_o \pm \omega_i)$.

The permitted grid frequency variation range in Brazil, under normal operating conditions, is 59.9 Hz to 60.1 Hz. In system disturbance situations, the frequency can vary from 59.5 Hz to 60.5 Hz, and thus, the maximum frequency fluctuation is $\Delta f = 1Hz$. To achieve sufficient gain across the entire operating frequency range $\omega_i = 2.\pi.\Delta f = 2\pi \; rad/s$. The following is the regulator design procedure.

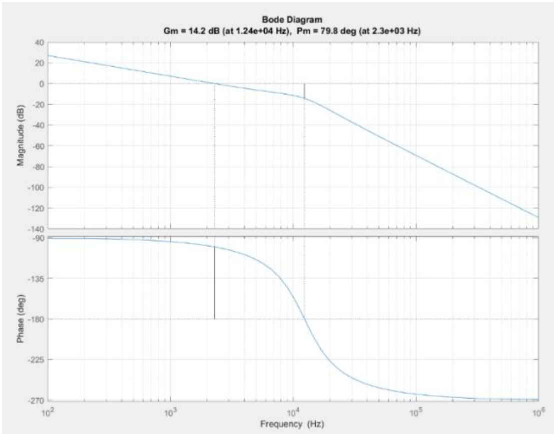

Figure 5(a): Frequency Response of the Uncompensated System

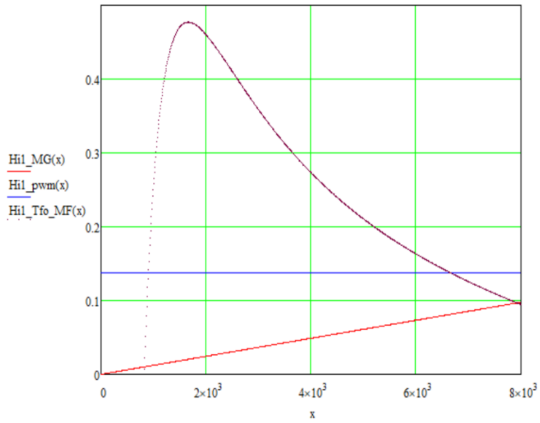

Figure 5(b): Block Diagram of Single-Phase Inverter Operating in Grid Follower Mode

Step 1: Specify the desired FTMA gain values at the fundamental frequency, T_{f_o}, the desired Minimum Phase Margin, and the desired Minimum Gain Margin.

- T_{f_o} is related to the steady-state error of the current injected into the grid;

-MF and MG are related to the dynamic response speed, robustness, and relative stability of the system;
For our inverter, we will choose:

- $T_{f_o} \geq 90\,dB$
- $MF \geq 45^{\circ}$
- $MG \geq 3\,dB$

Step 2: The choice of H_{i1} is directly linked to the choice of the gain crossover frequency of the compensated system. The equations are presented below, and Figure 12 shows the graph of H_{i1} versus the gain crossover frequency in each case:

- H_{i1} as a function of the gain at the fundamental frequency and the Phase Margin:

$$H_{i1\_T_{f_o}\_MF} = \frac{2.\pi.L_1.\left(f_r^2 - f_c^2\right)}{K_{PWM}.f_c} \cdot \frac{\pi.f_c^2 - \left(10^{\frac{T_{f_o}}{20}}.f_o - f_c\right).\omega_i.tg(MF)}{\left(10^{\frac{T_{f_o}}{20}}.f_o - f_c\right).\omega_i + \pi.f_c^2.tg(MF)}$$

- H_{i1} as a function of the MG Profit Margin:

$$H_{i1\_GM} = 10^{\left(\frac{MG}{20}\right)}.\frac{2.\pi.f_c.L_1}{K_{PWM}}$$

- H_{i1} as a function of the Switching Frequency:

$$H_{i1} < \frac{4.f_{sw}.L_1}{K_{PWM}}$$

From Figure 5(b), we can see that we can choose crossover frequencies up to approximately 8 kHz.

Step 3: Select an appropriate gain crossover frequency that satisfies all three H_{i1} conditions, i.e., falls within the region delimited by the H_{i1} curves. A higher value f_c improves dynamic performance and low-frequency gains. We will choose the gain crossover frequency of the compensated system as:

$$f_c = 7\,kHz$$

Step 4: Calculate the for the chosen crossover frequency:

$$K_p \cong \frac{2.\pi.f_c.(L_1 + L_2)}{H_{i2}.K_{PWM}} \Rightarrow K_p = 2.665$$

Step 5: Select a H_{i1} value within the demarcated region to satisfy the MF and MG requirements. For a fixed fc, increasing H_{i1} decreases the phase margin, but does not affect it. Therefore, while preserving the MF condition, a lower H_{i1} value is desirable to improve dynamic performance. From the graph, we will then adopt the following value for H_{i1}:

$$H_{i1} = 0.1$$

Step 6: Calculate the limits of K_r according to the requirements of T_{f_o} and MF. The upper limit of K_r is K_{r_MF} and the lower limit is K_{r_MF}.

$$K_{r\_T_{f_o}} = \left(10^{\frac{T_{f_o}}{20}}.f_o - f_c\right).\frac{2.\pi.(L_1 + L_2)}{H_{i2}.K_{PWM}} \Rightarrow K_{r\_T_{f_o}} = 147.18$$

The gain K_r as a function of the phase margin can be calculated by equation (2) above. Thus, taking $MF = 45^{\circ}$:

$$K_{r\_PM} = \frac{\pi.f_c.K_P}{\omega_i}.\frac{2.\pi.L_1.\left(f_r^2 - f_c^2\right) - H_{i1}.K_{PWM}.f_c.tg(MF)}{H_{i1}.K_{PWM}.f_c + 2.\pi.L_1.\left(f_r^2 - f_c^2\right).tg(MF)} \Rightarrow K_{r\_PM} = 2055.25$$

That way: $K_{r\_T_{f_o}} \leq K_r \leq K_{r\_MF} \Rightarrow 147{,}18 \leq K_r \leq 2055{,}25$

Step 7: The gain at the chosen frequency $f_c = 7{,}000Hz$ is $-8{,}55dB$. Let's analyze the gain required by the PR compensator to have this gain at this frequency:

$$20.log|G_i(j.2.\pi.7000| = 8{,}55dB \Rightarrow K_r = 1025.15$$

Step 8: Thus, the controller parameters are summarized below:

$$\begin{cases} K_P = 2.665 \\ K_r = 1025.15 \\ H_{i1} = 0.1 \end{cases}$$

Designed PR regulator:

$$G_i(s) = K_P + \frac{2.K_r.\omega_i.s}{s^2 + 2.\omega_i.s + \omega_o{}^2} \Rightarrow G_i(s) = \frac{2{,}665.s^2 + 12915.90.s + 142122.30}{s^2 + 12.566.s + 142122.30}$$

Step 9: The gain at the $f_c = 7000Hz$ chosen frequency is. Let's analyze the gain required by the PR compensator to have this gain at this frequency:

$$20.log|G_i(j.2.\pi.7{,}000| = 8.55dB \Rightarrow K_r = 1025.15$$

Step 10: The controller parameters are summarized below:

$$\begin{cases} K_P = 2.665 \\ K_r = 1025.15 \\ H_{i1} = 0.1 \end{cases}$$

PR Regulator Designed:

$$G_i(s) = K_P + \frac{2.K_r.\omega_i.s}{s^2 + 2.\omega_i.s + \omega_o{}^2} \Rightarrow G_i(s) = \frac{2.665.s^2 + 12915.90.s + 142122.30}{s^2 + 12.566.s + 142122.30}$$

The discretized controller using the Tustin method: $G_i(z) = \frac{2.66.z^{-2} - 5.33.z^{-1} + 2.67}{1.z^{-2} - 2.z^{-1} + 1}$

$$\Rightarrow v_r(k) = 2{,}67.e(k) - 5{,}33.\ e(k-1) + 2{,}66.e(k-2) + 2.v_r(k-1) - 1.v_r(k-2)$$

Step 11: Compensated system response.

We obtained the following parameters for the compensated system, as presented in Figure 6, and as follows:

- Gain Margin: 5.19dB
- Phase Margin: 45.9 °
- Mesh Gain @60Hz: 91.7dB
- Gain Crossover Frequency: 7kHz
- Phase Crossover Frequency: 12kHz

Notice that the parameters were within the desired values.

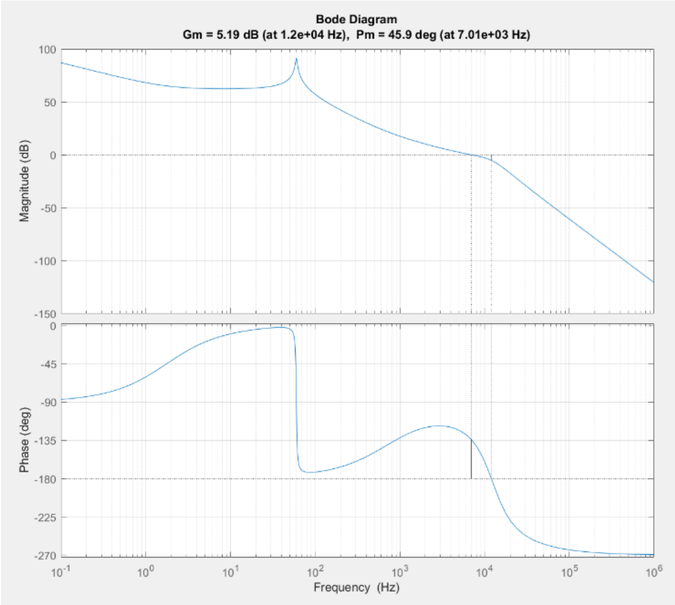

Figure 6 – Frequency response of the Compensated System.

6. Simulation Results – Grid – Following Inverter

In mains follower mode, the reference current is synchronized with the mains voltage via an EPLL. The reference current value is chosen so that the current injected into the grid is 18.18A, which corresponds to the 4kW of nominal power of the inverter. The signals were all adequate in the range (-1,1) through their respective full-scale gains for easy comparison. Figure 7(a) shows the mains voltage, the reference current, and the current injected into the mains. In the application of the microgrid, the power available on the bus by renewable sources will be converted into a reference current that will feed the inverter.

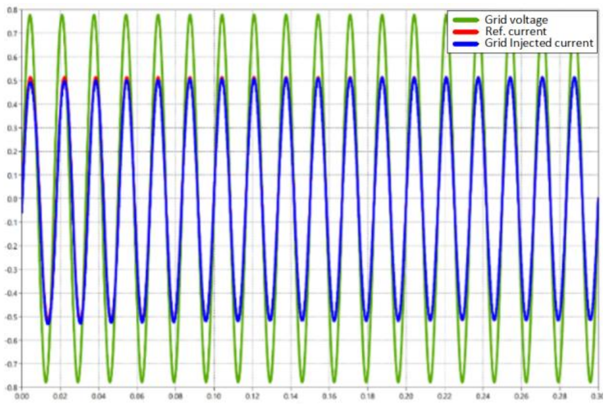

Figure 7(a): Network Voltage, Reference Current, and Current Injected into the Network

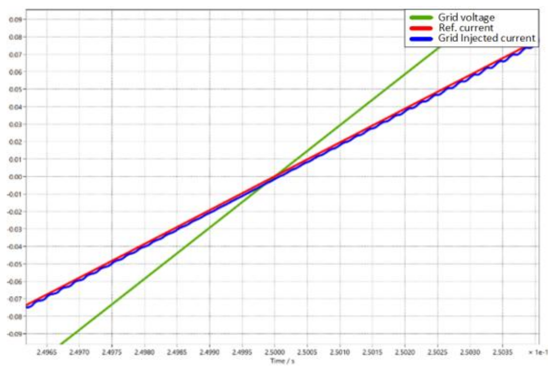

Figure 7(b): Close details between the voltage of the electrical network, reference current, and current injected into the network

Figure 7(b) shows the timing of the reference current with the sine of the network and the waveform of the injected current. In Figure 8(a), different network conditions were simulated for the observation of the injected current. During the interval from 0 to 0.3 s, the network was in good condition (220 V), during the interval from 0.3s to 0.6 s, there was a voltage drop to 170 V, and from 0.6 s to 0.9 s, the network voltage was present with harmonics (10% of 3rd harmonic plus 5% of 5th harmonic). Figure 8(b) shows how the THD of the current behaved during these intervals. During the first two intervals (0 – 0.6 s) the THD was practically constant at 0.8%. With the injection of harmonics into the network, the THD of the injected current rose to 3.34%, still below 5%.

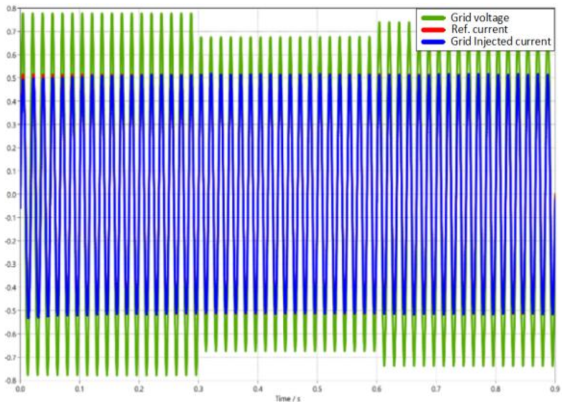

Figure 8(a): Network Voltage, Reference Current, and Current Injected into the Network

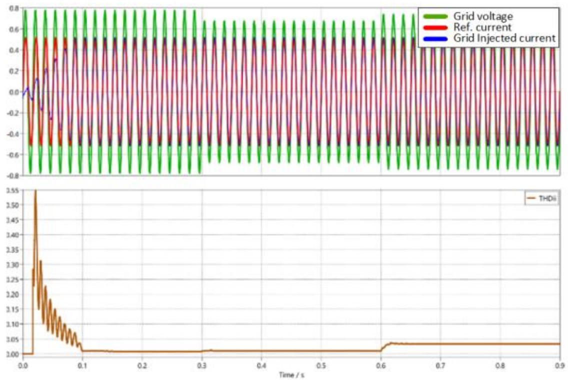

Figure 8(b): Close details between the voltage of the electrical network, reference current, and current injected into the network

Figure 9 shows the synchronism between the mains voltage and the injected current, their nominal effective values, and the THD of the waveforms.

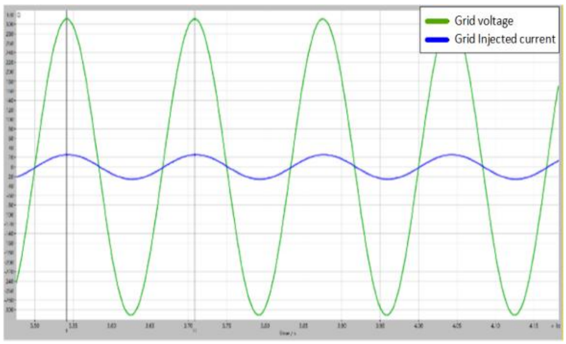

Figure 9(a): Network Voltage and Injected Current for normal grid

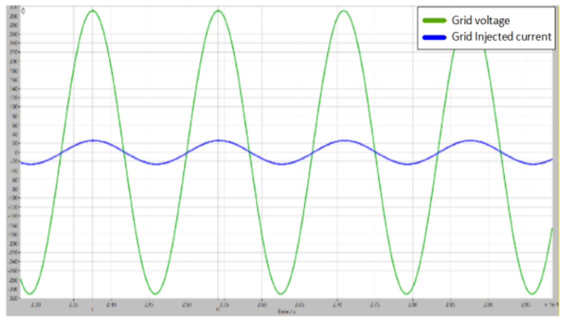

Figure 9(b): Network Voltage and Injected Current for weak grid

7. Modeling Inverter Grid - Forming

For the LCL filter grid-forming inverter, the open-loop transfer function is given by:

$$FTMA(s)=\frac{H_{i2}.K_{PWM}.G_i(s)}{s^3.\dfrac{L_1.L_2.C}{R_{nom}}+s^2.(\dfrac{L_2.C.H_{i1}.K_{PWM}}{R_{nom}}+L_1.C)+s.\left(\dfrac{L_1+L_2}{R_{nom}}+K_{PWM}.H_{i1}.C\right)+1}$$

The compensator used will be a PI controller $G_i(s)=K_P+\dfrac{K_I}{s}$.

Step 1: Determine the approximate value of the gain K_P as a function of the frequency of crossover gain:

$$K_p\cong\frac{\sqrt{\left(2.\pi.f_c.(\dfrac{L_1+L_2}{R_{nom}})-\dfrac{L_1.L_2.C}{R_{nom}}.(2.\pi.f_c)^3\right)^2+\left(1-L_1.C.(2.\pi.f_c)^2\right)}}{H_{i2}.K_{PWM}}$$

Step 2: Determine the gain K_I as a function of the gain T_{f_o} in the fundamental frequency and the crossing frequency:

$$K_{I\_T_{f_o}}=\frac{2\pi f_o}{H_{i2}.K_{PWM}}.\sqrt{\left(10^{\frac{T_{f_o}}{20}}\right)^2-1-\left(2\pi f_c.\left(\frac{L_1+L_2}{R_{nom}}\right)\right)^2}$$

Step 3: Determine the gain K_I as a function of the phase margin, the gain crossing frequency, and the H_{i1} gain:

$$K_{I\_MF} = 2\pi f_c . K_P . tg\left(arctg\left(\frac{2\pi f_c . \left(\frac{L_1 + L_2}{R_{nom}} + K_{PWM} . H_{i1} . C - (2\pi f_c)^2 . \frac{L_1 . L_2 . C}{R_{nom}} \right)}{(2\pi f_c)^2 . (\frac{L_2 . C . H_{i1} . K_{PWM}}{R_{nom}} + L_1 . C) - 1} \right) - MF \right)$$

Step 4: Choose a H_{i1} value and a gain crossing frequency that simultaneously satisfy the two previous equations: $K_{I\_T_{f_o}} = K_{I\_MF}$

The graph two allowed values of H_{i1} are plotted in Figure 10(a).

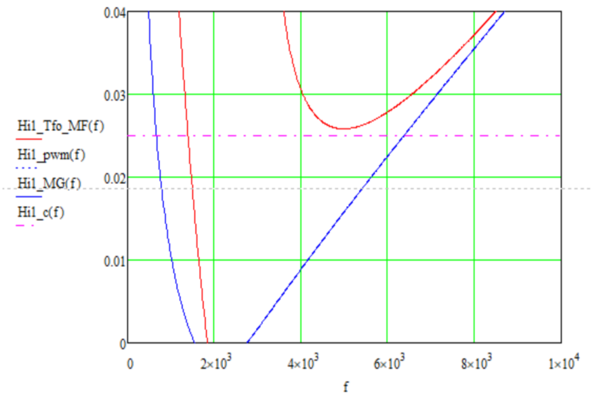

Figure 10(a): Possible Hi1 Values

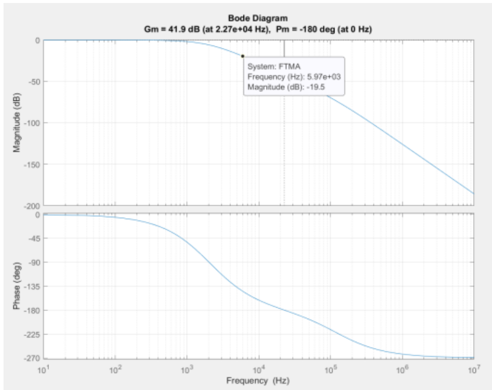

Figure 10(b): Frequency Response of the Uncompensated System

Step 5: From the previous chart, choose the desired performance parameters of the control loop:

$$- \; T_{f_o} \geq 40\,dB$$

$$- \; MF \geq 30^{o}$$

$$- \; MG \geq 3\,dB$$

From the graph in step 4, choose the value of H_{i1} and the gain crossing frequency:

$$H_{i1} = 0{,}025$$

$$f_c = 6\,kHz$$

Step 6: For the chosen crossing frequency and from step 2, we get the value of K_I. Let's adopt:

$$K_I = 37690$$

Step 7: Plot the frequency response of the uncompensated system and see how much the gain needed to be provided by the compensator is to leave the gain crossing frequency at the desired value:

$$Ganho_{PI} = 19.5dB$$

Step 8: For the chosen crossing frequency, we will determine the gain K_P to provide that gain:

$$20.\,log\left(\left|K_P + \frac{K_I}{j.\,2\pi f_c}\right|\right) = 11.9 \Rightarrow K_P = 6.038$$

Step 9: Trace the frequency response of the compensated system.

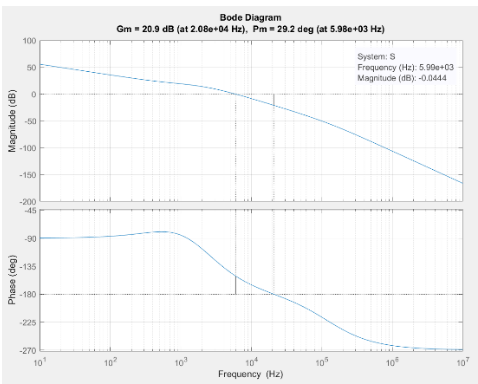

Figure 11 – Frequency Response of the compensated system.

Notice that the crossover frequency was exactly where we wanted it to be (6 kHz).

Step 10: Performance parameters of the designed control loop:
- Gain in fundamental frequency: $T_{f_o} = 40\,dB$
- Gain Margin: $MG = 20.9dB$
- Phase Margin: $MF = 29.2^o$

In summary: $H_{i1} = 0.025$, $K_I = 37{,}690$ and $K_P = 6.038$.
Designed PI Regulator:

$$G_i(s) = K_P + \frac{K_I}{s} \Rightarrow G_i(s) = 6.038 + \frac{37{,}690}{s}$$

The discretized controller using the Tustin method:

$$G_i(z) = \frac{(6.0568 - 6.0191.z^{-1})}{(1 - z^{-1})} \Rightarrow v_r(k) = 6.0568.e(k) - 6.0191.e(k-1) + v_r(k-1)$$

8. Simulation Results – Grid - Forming Inverter

Figure 12(a) shows the simulation result for linear loads. Every 0.2 s of the load on the inverter output was given a load step for the following percentages of the rated power: 100% - 50% - 1% - 100% -1% - 50% - 100%.

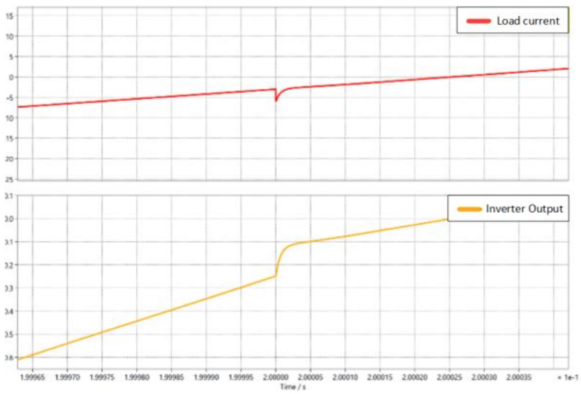

Figure 12(a): Inverter behavior for various load step scenarios

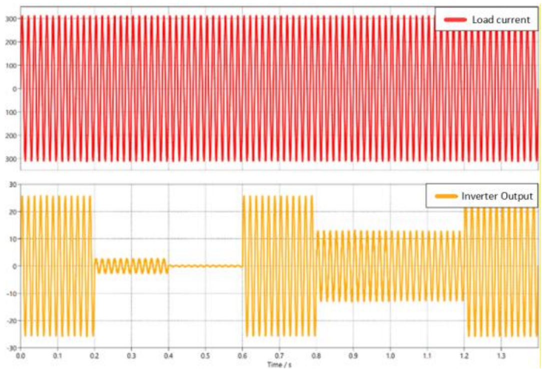

Figure 12(b): Detail of load step 100% - 50% for linear loads

Figure 12(b) shows the detail on the 100% step to 50% load. Figure 13(a) shows the simulation with a nonlinear load interspersed with a linear load, with changes in the same previous times. The sequence of the load steps occurs every 0.2s in the following sequence of load percentages: 100%(linear) – 10%(nonlinear) – 1%(linear) – 100%(linear) – 50%(nonlinear) – 50%(linear) – 100%(nonlinear).

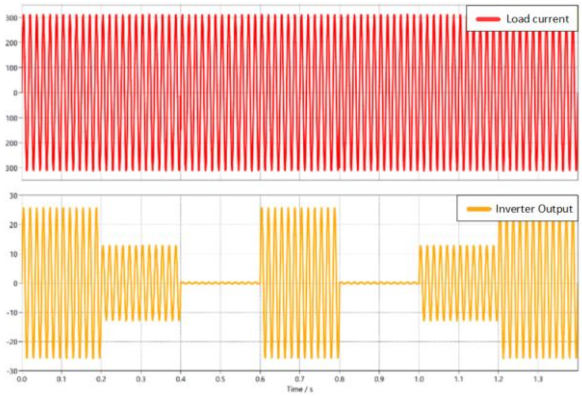

Figure 13(a): Inverter Behavior for Nonlinear Load: 100%(linear) – 10%(nonlinear) – 1%(linear) – 100%(linear) – 50%(nonlinear) – 50%(linear) – 100%(nonlinear)

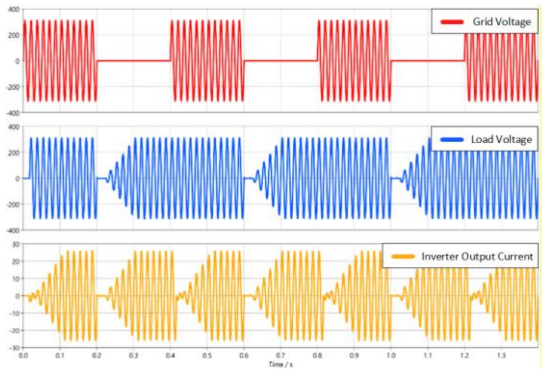

Figure 13(b): Switching between the states of the hybrid inverter

9. Hybrid Inverter

After analyzing the operation of each mode of the separate inverter, a code in C was made by joining the two algorithms, and a state machine was created so that the inverter can operate in both modes: grid follower and grid former. When the grid is present, the inverter operates as a grid follower, injecting power into the grid. When the grid is absent, after 1 cycle, the inverter now enters operating in grid-forming mode. A high-speed, 3-pole static switch is required at the common coupling point for switching modes and discharging power from the L2 inductor. A free-wheeling resistor is placed in parallel with the inductor for the discharge of this energy.
In Figure 13(b) below, every 0.2s, the state of the grid is inverted to visualize the behavior of the inverter. Note that when the grid is out, the inverter departs as a grid-forming device with a soft start to minimize *voltage and current* spikes.

10. Conclusions and Future Works

This work demonstrates a hybrid single-phase inverter that operates in both grid-forming and grid-following modes for residential microgrids, achieving continuous on-grid/off-grid operation through digital control. It is part of a complete project of a residential-sized microgrid that integrates renewable sources and battery storage through a DC bus, using PR/PI controllers with drop regulation to stabilize voltage/frequency and ensure reliable power sharing.

11. Bibliographic References

[1] PRIYADARSHI, N.; BHOI, A.K.; BANSAL, R.C.; KALAM A.; " DC-DC Converters for Future Renewable Energy Systems", Springer, 2022.

[2] BHASKAR M. S.; GUPTA N.; PADMANABAN S.; NIELSEN J. B. H.; SUBRAMANIAN U.; "Power Electronics for Green Energy Conversion", Jonh Wiley & Sons, 2022.

[3] KUMAR L. A.; ALEXANDER S. A.; RAJENDRAN M.; "Power Electronic Converters for Solar Photovoltaic Systems", Elsevier, 2021.

[4] PADMANABAN, S.; NITHIYANANTHAN, K.; KARTHIKEYAN, S. P.; NIELSEN, J. B. H.; "Microgrids", CRC Press, 2021.

[5] BEVRANI H., FRANÇOIS B., ISE T.; "Microgrid Dynamics and Control", John Wiley & Sons, 2017.

[6] PRIYADARSHI, N.; SANJEEVIKUMAR, P.; AZAM F.; BHARATIRAJA C.; SINGH R.; "Advanced Power Electronics Converters for Future Renewable Energy Systems", CRC Press, 2023.

[7] LUO F. L., YE H.; "Advanced DC/AC inverters - Applications in Renewable Energy", CRC Press, 2013.

[8] VUKOSAVIC, S.; "Grid-Side Converters Control and Design – Interfacing Between the AC Grid and Renewable Power Sources", Springer, 2018.

[9] SHAFIEE Q., NADERI M.; "Microgrids: Dynamic Modeling, Stability and Control", Jonh Wiley & Sons, 2024.

[10] RATUL R.A.; "Design and Simulation of a Hybrid Isolated DC Microgrid", Lambert, 2022.

[11] SILVA, R. C.; "Estudo e Desenvolvimento de um Conversor Formador de Rede Multiterminal". Dissertção de Mestrado, Universidade Federal de Minas Gerais, Julho de 2020.

[12] FEKIK A.; GHANES M.; DENOUN H.; "Power Electronics Converters and Their Control for Renewable Energy Applications", Elsevier, 2023.

[13] RUAN, X.; "Control Techniques for LCL – Type Grid – Connected Inverters", Springer.